JOURNAL OF CHEMICAL INFORMATION AND MODELING

Article

pubs.acs.org/jcim

Binding Selectivity Studies of Phosphoinositide 3-Kinases Using Free Energy Calculations

Dima A. Sabbah,[†] Jonathan L. Vennerstrom,[†] and Haizhen A. Zhong*[,‡]

[†]College of Pharmacy, University of Nebraska Medical Center, 986025 Nebraska Medical Center, Omaha, Nebraska 68198-6025, United States

[‡]DSC 362, Department of Chemistry, The University of Nebraska, 6001 Dodge Street, Omaha, Nebraska 68182, United States

Supporting Information

ABSTRACT: Phosphoinositide 3-kinases (PI3Ks) and their phosphatidylinositol 3,4,5-triphosphate (PIP_3) products regulate a variety of cellular processes. Of these, PI3Kα is an attractive target for anticancer drug design. Mutations in the PI3Kα kinase domain alter the mobility of the activation loop resulting in gain of function. We employed molecular dynamics (MD) simulations-based energetic analysis using molecular mechanics/generalized born surface area (MM/GBSA) for PI3Kα and -γ. MD simulations were carried out for PI3K models based on the RESP (restrained electrostatic potential) and quantum mechanics (QM)-polarized ligand docking (QPLD)-derived partial charges. Computational alanine scanning was also used to evaluate the contributions of key binding residues to ligand binding. Our results show that both RESP and QPLD charge models of PI3Kα and PI3Kγ provide similar performance in MD simulations. For example, the predicted RESP and QPLD free energies of −9.5 and −9.3 kcal/mol for LY294002 binding to PI3Kγ and −10.9 and −11.7 kcal/mol for wortmannin binding to PI3Kα are in good agreement with experimental values. A significant loss in binding free energy was observed when hydrophobic residues were mutated to alanine, suggesting that specific hydrophobic interactions are important to optimal ligand binding. MM/GBSA calculations suggested that residues Ser774, Gln859, and Ile932 of PI3Kα might be used to design H1047R mutant-specific ligands, whereas Lys890 of PI3Kγ can be used for ligand design targeting PI3Kγ.

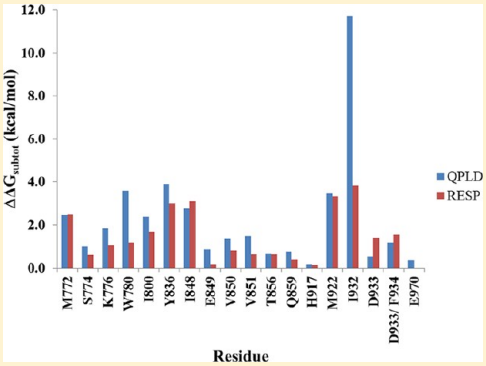

1. INTRODUCTION

Phosphatidylinositol 3-kinases (PI3Ks) phosphorylate phosphatidylinositol 4,5-biphosphate (PIP_2) to generate phosphatidylinositol 3,4,5-triphosphate (PIP_3), an important second message coordinating the activities of PI3K downstream effectors such as AKT. The activation of PI3K/AKT signaling triggers cell proliferation, growth, angiogenesis, and metastasis. Aberrations in the PI3K/AKT pathway have been observed in a number of human cancers.[1] There are three families of class IA PI3Ks, each with distinct substrate specificity and primary structures, p110α, p110β, and p110δ isoforms, encoded by PIK3CA, PIK3CB, and PIK3CD, respectively. PI3Kγ, the only class IB PI3K protein, is a structural homologue of PI3Kα. PI3Kα and PI3Kβ are ubiquitous in mammalian tissues, whereas PI3Kδ and PI3Kγ are mainly present in leukocytes.[2] PIK3CA, the coding gene of PI3Kα, is mutated and amplified in numerous human tumors. PI3Kα is the principal isoform regulating tumor growth and proliferation, whereas PI3Kγ mediates inflammatory pathways and is considered as a target for rheumatoid arthritis and asthma.[3] Numerous inhibitors have been reported to inhibit both PI3Kγ and PI3Kα; only a few of these are α-isoform selective. Selective inhibition of PI3Kα has been considered as a viable approach for cancer treatment. Thus, to assist future structure-based drug design, we investigated binding site differences between these two PI3K isoforms to identify residues associated with selective ligand binding. The selection of PI3Kα and γ was also based on the availability of crystal structures for these two isoforms.

PIK3CA mutations and amplification have been found in colon, breast, brain, and endometrial cancers.[4,5] The majority of these mutations are located in the helical (E542K and E545K) and the kinase (H1047R) domains. These "hot-spot" mutations enhance the in vitro kinase activity of PI3Kα, a phenomenon described as "gain-of-function."[6,7] Using human mammary epithelial cells (HMEC), Liu et al. found that mutations of E545K and H1047R activated the AKT signaling cascade and produced genetic transformations.[8] Although PIK3CA mutations have been found in more than 30% of colon and breast cancer patients,[4] only 7.1% of gastric cancer patients carried these same mutations; however 67% of the latter patients had amplifications in PIK3CA,[9] indicating that inhibition of wild-type PI3Kα may be a viable approach to suppress gastric tumor cell growth. In patients with primary colorectal adenocarcinomas (CRC) and associated hepatic metastases, 17 out of 21 were characterized with variance in EGFR mutational status between the primary CRC and liver metastases; in this same patient population, only 4/21 had mutational variability. No

Received: June 29, 2012
Published: November 17, 2012

variants were detected in PIK3CA codons 542, 545, and 1047,[10] indicating that inhibition of the H1047R mutant of PI3Kα would be effective in patients with both primary tumors and metastases.

To guide PI3K inhibitor design, we employed computational methods to investigate the role of individual residues in ligand binding. Han and Zhang carried out molecular dynamic (MD) simulations of the kinase domains of the α and γ isoforms of PI3K and observed that residues Trp780 and Asn782 in PI3Kα (Trp812 and Glu814 in PI3Kγ, respectively) could confer isoform specificity.[11] Our docking studies indicated that structural differences in the kinase loop and residues Gln859, Ser854, Tyr836, and Ser774 of PI3Kα could be exploited to design isoform-specific or mutant-active inhibitors.[12]

The PI3Kα D915A mutant and D933A/F934A double mutant both show a complete loss of kinase activity, whereas the E970A mutant had little effect.[13] PI3Kα gatekeeper mutants I848A, I848G,[14] I848L, I848S, and I848 V[15] showed losses in catalytic activities, whereas mutant H1047R enhanced the lipid kinase activity (relative to the wild-type).[6,16] Additional mutations in the H1047R strain led to three different outcomes: unchanged, potentiated, or weakened kinase activities. For example, the C838A, C838T, and G837M double mutants retained the same activities as H1047R; the S854A and G837N mutants potentiated the kinase activities of H1047R, and the L814C, L814N, I800L, I800M, and I848V mutants weakened or abolished the activity of H1047R. Various PI3K inhibitors have a range of potencies against these double mutants: the PI3K inhibitors PIK-90, PIK-93, PI-103, PP-110, PW-12, and BEZ-235 are less potent against the I848V and I800M mutants, whereas PIK-90, PIK-93, and PP-110 are more potent against the H1047R mutant.[15] The potentiating or weakening effects of these binding residue mutations, however, were observed only for the H1047R mutant, and not for the wild-type PI3Kα.

To design isoform- or mutant-selective inhibitors, it is necessary to understand the effects of residue mutations in the enzyme active site. In this work, we systematically investigated how active site mutations affected ligand binding for the wild-type (WT) and H1047R mutant (MUT) PI3Kα, and PI3Kγ. We employed molecular dynamics (MD) simulations-based molecular mechanics/generalized Born surface area (MM/GBSA) calculations and computational alanine scanning.[17,18] To investigate the effect of charge models on ligand binding in our MD simulations, we applied conventional RESP (restrained electrostatic potential) charges and quantum mechanics (QM)-polarized ligand docking (QPLD)-derived partial charges for bound ligands. QPLD-derived partial charge models have shown improvements in predicting docking conformations[19] and for estimating the binding free energies of DNA/ligand interactions.[20] However, no protein−ligand interactions based on the QPLD-based charge model have been reported. To our best knowledge, this is the first QPLD-based MM/GBSA calculation for kinase/ligand interactions.

2. COMPUTATIONAL METHODS

2.1. Preparation of Isoforms. The X-ray crystal structures of apo PI3Kα (PDB ID 2RD0),[16] the mutant (H1047R) PI3Kα/wortmannin complex (PDB ID 3HHM),[6] and the PI3Kγ/LY294002 complex (PDB ID 1E7 V)[21] were retrieved from the RSCB Protein Data Bank. The wortmannin coordinates of 3HHM were adopted to 2RD0 and used as a ligand. Four missing sequences in 2RD0 and 3HHM were fixed as described[12] using the homology module in MOE.[22]

2.2. Restrained Electrostatic Potential (RESP) Charge. The RESP partial charges for wortmannin were developed as follows. First wortmannin was optimized using HF/6-31G* ab initio calculations with Gaussian 03.[23] Then, the RESP charges were derived using the ANTECHAMBER script in AMBER10.[24] The atom types and the stretching, bending, dihedral, and improper dihedral parameters for both wortmannin and LY294002 were assigned based on the Generalized AMBER Force Field (GAFF).[24] The atom types and the atomic partial charges of these two ligands are listed in Supporting Information Tables 1S and 2S.

2.3. Quantum Mechanics Polarized Ligand Docking (QPLD)-Based Charges. In contrast to the RESP charges of a ligand calculated in a vacuum, QPLD-based partial charges are calculated in the environment of a protein structure. QPLD charges were developed using the QPLD protocol in the Schrödinger software suite.[25] Wortmannin was docked to PI3Kα wt, PI3Kα H1047R mutant, or PI3Kγ, and the resulting protein/ligand complexes were optimized with wortmannin treated by the QM approach and the protein treated by the molecular mechanics (MM) method using the QSite program. The QM/MM procedure determines a new set of atomic partial charges for the ligand based on QM calculations and takes into account the protein that was minimized with the MM force field. The minimized ligands (in the protein environment) were redocked to the protein active site and the docked pose with the lowest root-mean-square deviation (RMSD) from the reference was adopted and its partial charges were used for MD simulations.

2.4. Molecular Dynamics (MD) Simulations. Established procedures[12,18] for MD simulations were carried out using the AMBER 10 package[24] with the AMBER 99SB force field.[26] Briefly, residues Asp and Glu were assigned to −1 charges, and Lys and Arg were assigned +1 charges. The orientation of Asn, Gln, and His side chains were optimized to maximize H-bond interactions using the Protein Preparation Wizard in Schrödinger.[25] Each system was neutralized with sodium ions and soaked in a rectangular box of TIP3P water molecules[27] extended 10 Å away from any protein atom: 6 Na^+ and 1151 water molecules were added to 1E7 V (box size 68 × 69 × 80 Å for both RESP and QPLD charge models); 1 Na^+ and 5562 water molecules were added to 3HHM (box size 84 × 83 × 94 Å for both RESP and QPLD charge models); and 2 Na^+ and 6277 water molecules were added to 2RD0 (box size 83 × 83 × 98 Å for both RESP and QPLD charge models). Each system was subjected to a 1000 step minimization using the steepest descent algorithm to reduce the steric clashes, followed by a heating process for 30 ps from 10 to 300 K, and an equilibration for 100 ps at 300 K. The production simulations were carried out using the NPT ensemble with a time step of 1 fs and 4000 snapshots were collected during 4000 ps. For the 3HHM RESP model, a 12 ns simulation was carried out and the last 4 ns snapshots were used to obtain free energy and RMSD data. The 10 Å nonbonded cutoff was set to define the van der Waals interaction, and the particle mesh Ewald (PME) method was used to describe long-range electrostatic interactions.[28] All bonds involving hydrogen atoms were constrained using the SHAKE algorithm. Constant temperature and pressure (300 K/1 atm) were maintained by using Langevin dynamics to regulate temperature with a pressure relaxation time of 1 ps.

After MD simulations, the RMSDs of the backbone atoms for six model systems (3 proteins in two charge models) were obtained using the PTRAJ module in the AMBER 10 package to monitor stability of the protein systems.

2.5. Free Energy Calculations and Computational Alanine Scanning. The GBSA (molecular mechanics/Generalized Born surface area) method was used to calculate the free energy of binding (ΔG_{bind}).[29,30] The free binding energy can be estimated using Eq. 1

$$\Delta G_{binding} = \Delta G_{water}(complex) - [\Delta G_{water}(protein) + \Delta G_{water}(ligand)] \quad (1)$$

where $\langle G_{water} \rangle$ is the average free energy of the system calculated by Eq. 2

$$\langle G_{water} \rangle = \langle E_{bond} \rangle + \langle E_{angle} \rangle + \langle E_{torsion} \rangle + \langle E_{electrostatic} \rangle + \langle E_{vdw} \rangle + \langle G_{GB} \rangle + \langle G_{SA} \rangle - TS \quad (2)$$

The broken brackets, $\langle\rangle$, indicate that the free energy and the individual energetic components are average values of all snapshots collected over the 4 ns simulation period. Bond, angle, torsion, electrostatic, and vdw energy terms were calculated based on gas phase geometries. Solvation free energies were calculated based on polar (G_{GB}) and nonpolar (G_{SA}) energies. The polar term was evaluated using the Generalized Born theory (GB program in AMBER package)[31] and the nonpolar contributions due to solvation were estimated with the program MSMS.[32] The average entropy, S, was estimated using NMODE module[33,34] based on 10 snapshot configurations. All energy components and solvation contributions were calculated using 4 ns MD extracted trajectories for the ligand/protein complexes.

To investigate the impact of mutational effects on ligand binding, each residue within 4.5 Å of the bound ligands was computationally mutated to alanine using the MM/GBSA method. The free energy changes ($\Delta\Delta G_{bind}$) were defined as ΔG_{bind} (mutant) − ΔG_{bind} (wild-type) for a potential mutation from wt to mut. A positive $\Delta\Delta G_{bind}$ indicates that ligand binding to the wild-type protein is more favorable (i.e., less favorable to the mutant), as ΔG_{bind} (wild-type) is more negative. On the other hand, a mutation resulting in a more negative $\Delta\Delta G_{bind}$ is considered to be more favorable.

3. RESULTS AND DISCUSSION

3.1. Molecular Dynamics (MD) Simulations. The root-mean square deviations (RMSDs) of all three proteins (WT PI3Kα, 2RD0; MUT H1047R PI3Kα, 3HHM; and PI3Kγ/LY294002 complex, 1E7V) under two charge models were calculated as a function of time after a backbone least-squares fit. Supporting Information Figure 1S shows that stable RMSD profiles were observed in all simulations: the last 4 ns of the 3HHM (RESP) and other PI3Kα models (2RD0 in both charge models and 3HHM in QPLD model) showed similar stabilities. In reference to the starting crystal structure backbone atoms, the average RMSDs of all six models showed that for wortmannin binding to WT PI3Kα, the QPLD charge model offers trajectories with less deviation to the starting structure, whereas for the RESP charge model, the RMSDs are smaller in the H1047R mutant and the PI3Kγ models. The standard deviations of the PI3Kα H1047R MUT and the PI3Kγ models were lower than those derived from the QPLD charge model, whereas the QPLD charge model generates a slightly smaller standard deviation that that of the wild-type PI3Kα model (Table 1). Therefore, although the QPLD-based charge model has found great success in ligand docking[19] and DNA/ligand interactions,[20] it does not offer a noticeable improvement over the RESP charge model in terms of the RMSDs of trajectories of these protein/ligand interactions, presumably because of hydrophobic binding pockets in kinases.

Table 1. Average and Standard Deviations (SD) of RMSDs of MD-Generated Trajectories for All Three Proteins in Two Different Charge Models (2RD0 for wt-PI3Kα/wortmannin, 3HHM for H1047R mutant PI3Kα/wortmannin, and 1E7V for PI3Kγ/LY294002)

	RESP charge models			QPLD charge models		
	2RD0	3HHM	1E7V	2RD0	3HHM	1E7V
mean	2.4	2.0	1.7	2.1	2.7	2.0
SD	0.3	0.5	0.2	0.2	0.3	0.3

3.2. Free Energy Calculations and Model Validation. To determine which factors are more important for ligand binding in the six model systems, binding free energies and individual energy components were determined using the MM/GBSA method (Table 2). Model validation was accomplished by comparing our calculated free energy values (ΔG_{bind}) for the PI3Kγ/LY294002 complex (−9.5, and −9.3 kcal/mol for the RESP and QPLD models, respectively) to the apparent PI3Kγ K_d of 210 nM for LY294002, which corresponds to a calculated ΔG_{bind} of −9.2 kcal/mol.[21] This ΔG_{bind} was calculated based on the formula of $\Delta G_{bind} = RT \ln(K_d)$.[35,36] Our free energy calculations show that both QPLD and RESP charge models are able to predict the experimentally determined free energy of binding (ΔG_{bind}) of a protein/ligand complex (1E7V/LY294002). It is conceivable that the HF/6-31G* level of theory overestimates the in vacuum calculated electrostatic potential and thus can de facto effectively polarize solutes. The effectiveness of applying RESP partial charges to small molecules has been demonstrated in the influenza A virus neuraminidase[37] and DNA/netropsin[38] simulations.

Wortmannin is a first-generation nonselective PI3K inhibitor. It inhibits both PI3Kα and γ with IC_{50} values of 12 and 4.2 nM, respectively.[21] The ΔG_{bind} of wortmannin (−10.9 and −11.7 kcal/mol for the respective RESP and QPLD models) to WT PI3Kα are in good agreement with experimental data ($\Delta G_{bind\ (exp)}$ of wortmannin: −10.9 kcal/mol). For the same charge model, the ΔG_{bind} in the H1047R mutant model is slightly more negative than that in the WT model, indicating that wortmannin binds more tightly to the mutant protein. This is in accord with the fact that H1047R mutant caused a gain-of-function in the lipid kinase activities and with our previous docking affinity prediction that wortmannin binds more tightly to the mutant.[12,39]

Analyses of the energy components for all six models reveal that the intermolecular van der Waals force (E_{vdw}) is the biggest contributor for ligand binding to PI3K (Table 2). Because of the hydrophobic PI3K binding pocket, this outcome is not surprising; more than half of the residues within 4.5 Å of wortmannin or LY294002 are hydrophobic.[12] Both E_{vdw} and the nonpolar solvation contribution ΔG_{SA} drive the interactions between PI3Ks (both α and γ isoforms) and their ligands. The value of ΔG_{SA} is proportional to the solvent accessible surface areas that are buried during the complexation process. The favorable effect of burying hydrophobic residues during ligand

dx.doi.org/10.1021/ci3003057 | J. Chem. Inf. Model. 2012, 52, 3213−3224

Table 2. Energy Components and Binding Free Energies for Three Proteins in Two Different Charge Models (2RD0 for WT PI3Kα/wortmannin, 3HHM for H1047R MUT PI3Kα/wortmannin, and 1E7V for PI3Kγ/LY294002)

	RESP charge models			QPLD charge models		
	2RD0 (WT)	3HHM (MUT)	1E7V	2RD0 (WT)	3HHM (MUT)	1E7V
ΔE_{elec}	−19.0 ± 4.7	−28.4 ± 3.8	−6.8 ± 3.0	−20.4 ± 3.6	−35.7 ± 4.4	−21.9 ± 3.1
ΔE_{vdw}	−50.3 ± 2.9	−51.0 ± 2.8	−35.2 ± 2.8	−49.4 ± 2.6	−50.6 ± 2.7	−39.3 ± 1.8
ΔG_{SA}	−5.9 ± 0.3	−6.2 ± 0.2	−4.4 ± 0.3	−5.8 ± 0.2	−6.3 ± 0.2	−5.2 ± 0.2
ΔG_{GB}	39.0 ± 4.6	40.3 ± 3.0	14.9 ± 3.0	32.9 ± 3.2	46.0 ± 4.0	28.7 ± 2.3
ΔG_{solv}	33.0 ± 4.5	34.1 ± 3.0	10.6 ± 2.8	27.1 ± 3.1	39.7 ± 3.9	23.5 ± 2.3
ΔG_{subtot}	−36.3 ± 2.8	−45.3 ± 2.7	−31.4 ± 2.9	−42.7 ± 2.7	−46.6 ± 2.7	−37.6 ± 1.9
$-T\Delta S$	25.4	32.6	21.9	31.0	34.0	28.3
ΔG_{bind}	**−10.9**	**−12.7**	**−9.5**	**−11.7**	**−12.6**	**−9.3**

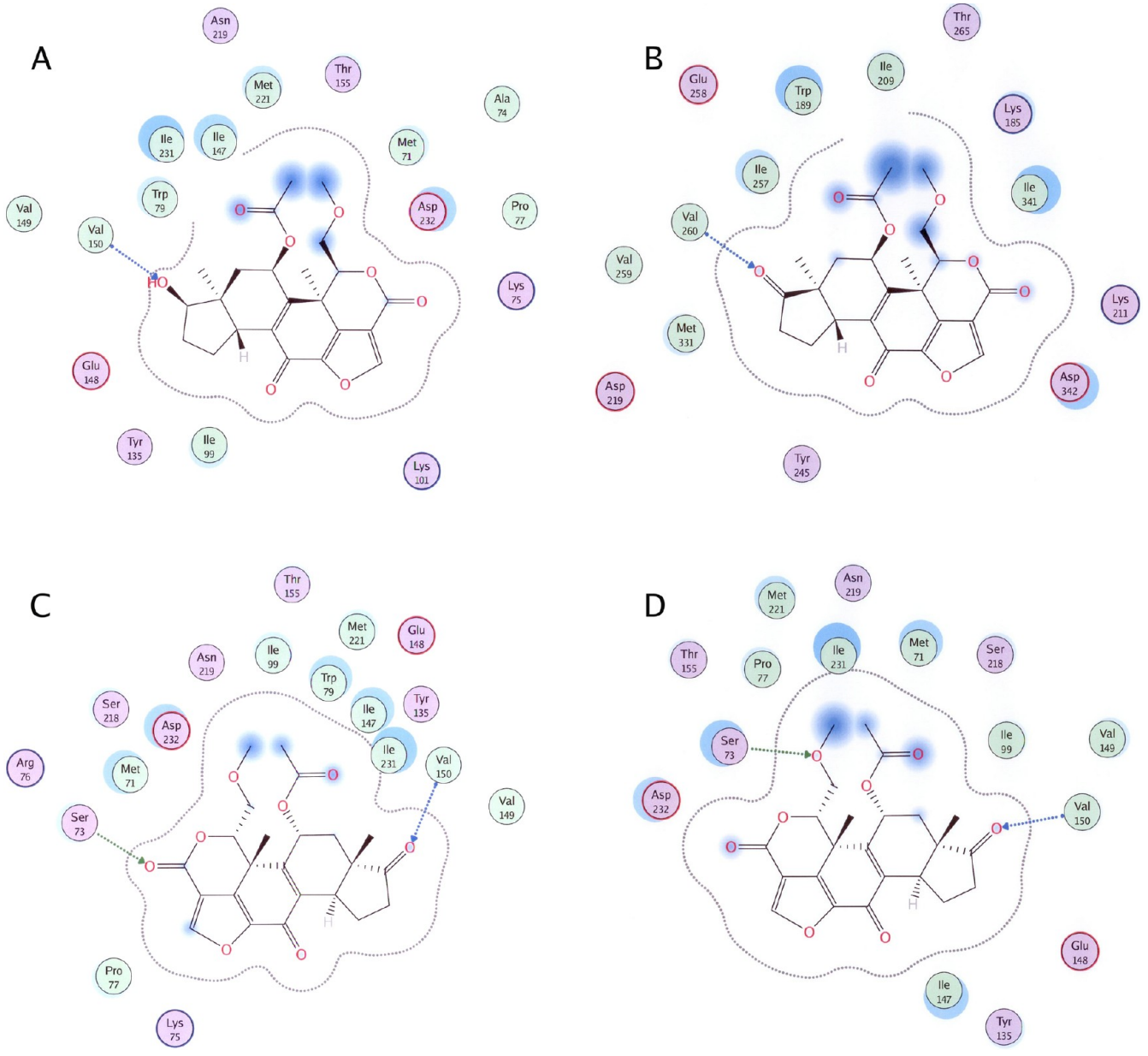

Figure 1. Binding interactions between PI3K/ligand; (A) 2RD0/wortmannin (wt RESP model), (B) 2RD0/wortmannin (wt QPLD model), (C) 3HHM/wortmannin (MUT QPLD model), and (D) 3HHM/wortmannin (MUT RESP model). For A, C, and D, 701 was added to given residue numbers to match residue numbers in PDB; for B, addition of 591 was needed to match residue numbers in PDB. Color codes: red circle, acidic residues; blue circle, basic residues; pink dots, polar residues; green dots, hydrophobic residues; blue dash line, backbone H-bonds; green dash line, side chain H-bonds.

dx.doi.org/10.1021/ci3003057 | J. Chem. Inf. Model. 2012, 52, 3213−3224

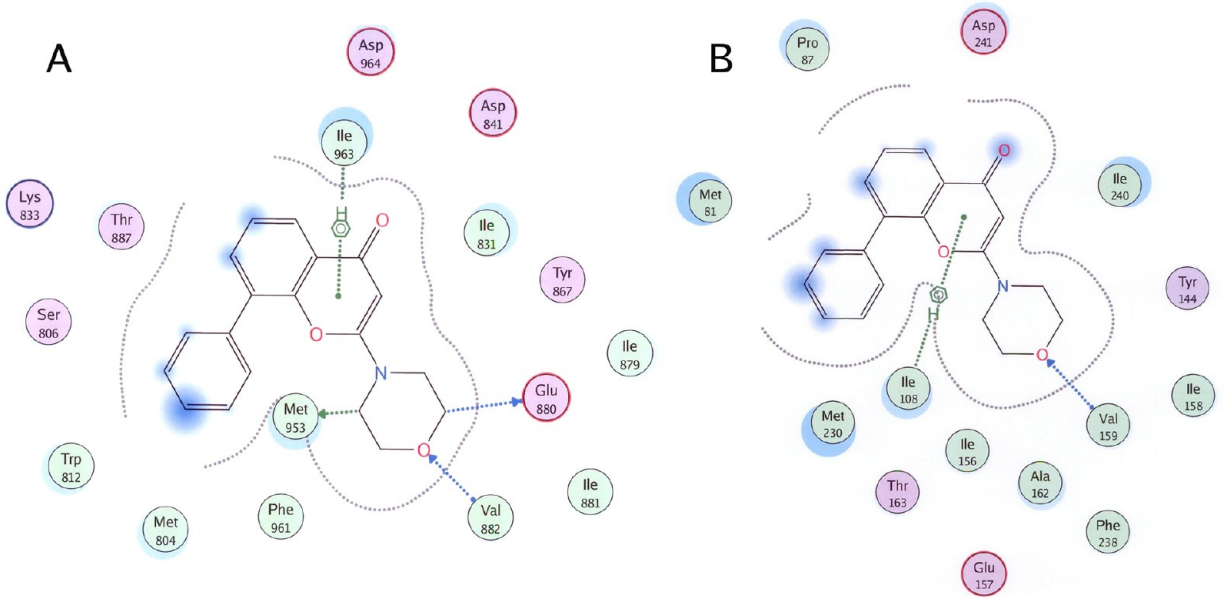

Figure 2. Binding interactions between 1E7V/LY294002: (A) X-ray native structure, (B) QPLD model. Adding 723 to the given residue numbers matched those in the PDB. Color codes: red circle, acidic residues; blue circle, basic residues; pink dots, polar residues; green dots, hydrophobic residues; blue dash line, backbone H-bonds; green dash line, side chain H-bonds.

binding is slightly larger in PI3Kα than in PI3Kγ. The contributions of ΔE_{vdw} and ΔG_{SA} are comparable in the RESP and the QPLD charge models.

The most noticeable difference between these two charge models and between the α and γ isoforms lies in electrostatic interactions. The RESP charge model appears to underestimate electrostatic contributions for all three protein model systems (PI3Kα WT, H1047R MUT, and PI3Kγ, Table 2). Charged residues within 4.5 Å of wortmannin in the WT PI3Kα binding pocket are Lys776, Lys802, Glu849, and Asp933 (Figure 1A). In the QPLD model, Asp810 was drawn closer to the active site, resulting in a larger electrostatic contribution (Figure 1B). Mutation of His1047 to Arg (3HHM model) in the mutant results in stronger electrostatic interactions (i.e., more negative numbers) and allows the formation of an additional H-bond with Ser774 for ligand binding; thus $\Delta E_{electrostatic}$ for 3HHM and 2RD0 is −28.4 and −19.0 kcal/mol, respectively. Because of an increase in charge potential in the 3HHM model, it is reasonable to observe a larger electrostatic contribution of −35.7 versus −28.4 kcal/mol in the QPLD vs RESP charge models. In the QPLD model, wortmannin in the H1047R PI3Kα complex is surrounded by charged residues Lys776, Arg777, Glu849, and Asp933 (Figure 1C), whereas in the RESP charge model, only Glu849, and Asp933 (Figure 1D) are within 4.5 Å of the ligand. The presence of two positive charged residues (Lys776 and Arg777) increases the positively charged potential, allowing more favorable electrostatic interactions with the partially negatively charged oxygen atoms of wortmannin. Although the individual energy components varied between different charge models, the binding free energies were very similar. This additive characteristic has also been observed in free energy calculations based on the free energy perturbation method.[40,41]

Electrostatic and VDW contributions are even more significant in the QPLD model of the PI3Kγ/ LY294002 (1E7V model). The 1E7V active site contains charged residues Lys833, Asp841, Glu880, and Asp964 (Figure 2A). These charged residues suggest that the QLPD charge model based on the protein environment would perform better than the RESP charge model where partial charges are developed based on an isolated ligand. This prediction is consistent with what we have observed in our previous DNA/duocarmycin studies where DNA carries multiple charged phosphate groups.[20] This is exactly what we found with PI3Kγ; the contribution of electrostatic interactions was greater in the QPLD model (−21.9 kcal/mol) than that in the RESP (−6.8 kcal/mol). However, it is interesting to observe that during the MD simulations, the movement of charges residues resulted in a conformation at the fourth ns snapshot with only two charged residues retained: Glu880 and Asp964 in the QPLD model, and Glu880 in the RESP charged model. Inspection of the electrostatic map of PI3Kγ (1E7V) of these two charged models showed that the QPLD model contained a H-bond donor region (blue region surrounding Asp964, Figure 3B) because of the presence of Asp964, allowing electrostatic attraction with a H-bond acceptor of the carbonyl oxygen in LY294002. Such an interaction was absent in the RESP charge model (Figure 3).

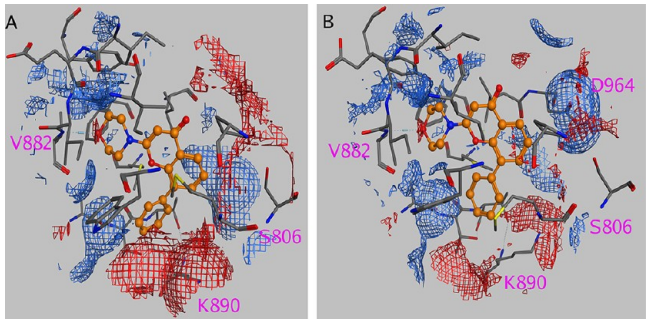

Figure 3. Electrostatic surface of the binding pockets of PI3Kγ/ LY294002: (A) RESP charged model and (B) QPLD charged model. Color code: H-bond acceptor, red; and H-bond donor, blue. The electrostatic surfaces were made with the MOE program.

dx.doi.org/10.1021/ci3003057 | J. Chem. Inf. Model. 2012, 52, 3213−3224

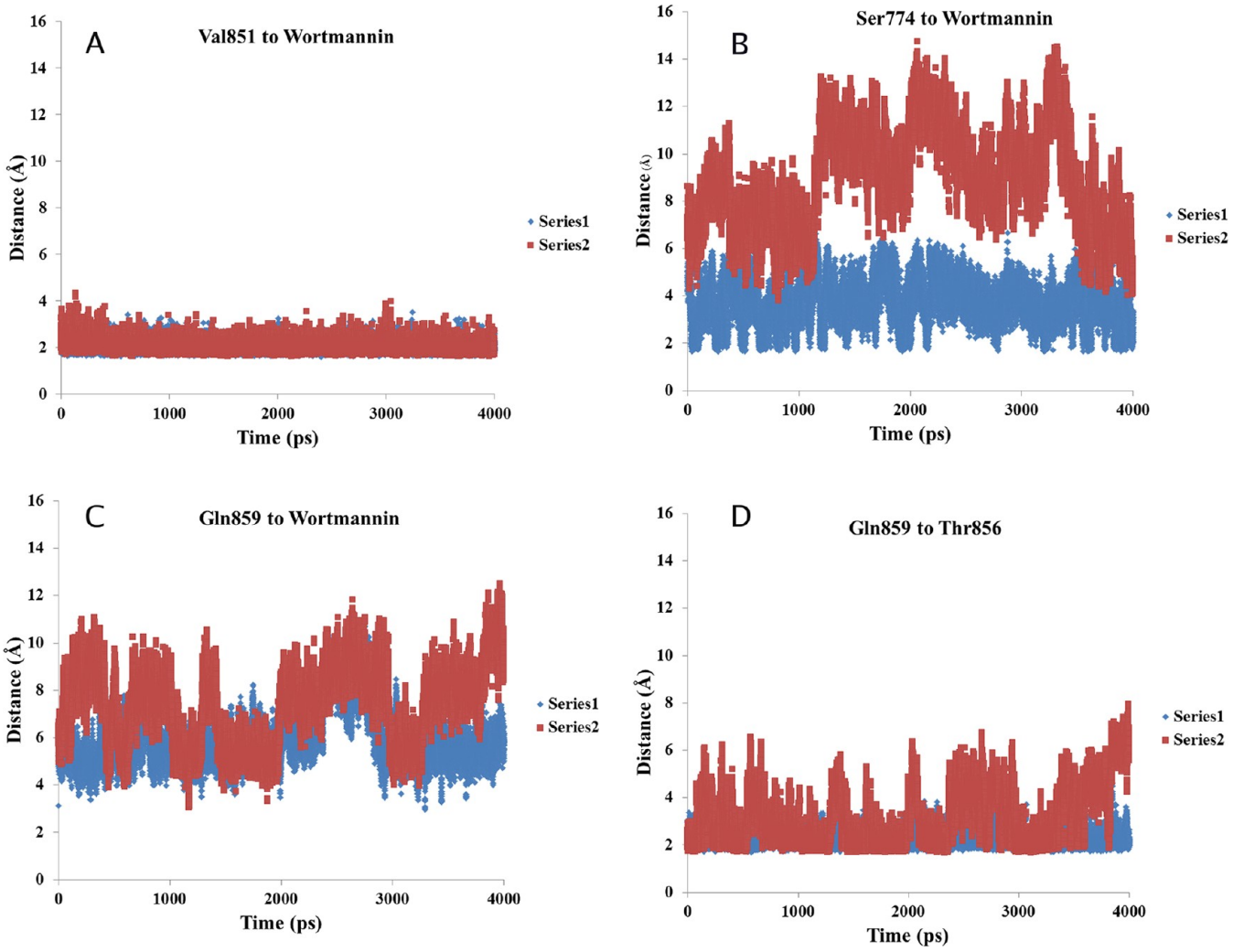

Figure 4. Distance proteins and ligands: (A) distance between Val851 NH of PI3Kα and wortmannin O6 (RESP models), series 1 (blue, MUT model, 2.0 ± 0.2 Å), series 2 (red, wt model, 2.1 ± 0.2 Å); (B) distance between Ser774 OH of PI3Kα and wortmannin O8 (RESP models), series 1 (blue, MUT model, 3.7 ± 0.9 Å), series 2 (red, wt model, 8.9 ± 2.1 Å); (C) distance between Gln859 NE2 of PI3Kα and wortmannin O7 (RESP models), series 1 (blue, MUT model, 5.9 ± 1.1 Å), series 2 (red, wt model, 7.3 ± 1.6 Å); and (A) distance between Gln859 NH and Thr856 OG1 of PI3Kα (QPLD models), series 1 (blue, MUT model, 2.2 ± 0.3 Å), series 2 (red, wt model, 3.1 ± 1.2 Å).

3.3. Mutant- or Isoform-Specific Binding. All six models have H-bond interactions between Val851 (PI3Kα wt or MUT), or Val882 (PI3Kγ) and ligand (wortmannin or LY294002). The distance between the Val851 backbone NH and the O6 of wortmannin was stabilized around 2.0 Å for both the wt and MUT PI3Kα models (Figure 4A). This explains the lack of selectivity of many PIK inhibitors that were designed to target PI3Kα Val851 (or Val882 in the γ-isoform). In the RESP model, the Ser774 in the PI3Kα MUT forms a stable H-bond with a wortmannin oxygen with a distance of 3.7 ± 0.9 Å. The distance for the same pair of atoms in the WT PI3Kα was 8.9 ± 2.1 Å. Therefore, our data suggests that Ser774 can be used to design mutant-specific inhibitors of PI3Kα. Gln859 in the MUT model is closer to the wortmannin O7 (distance, 5.9 ± 1.1 Å) than that in the WT (distance, 7.3 ± 1.6 Å, Figure 4C). In the MUT (RESP model), the distance between Gln859 and wortmannin was around 4 Å for more than half of the simulations; in other words, the H-bonds between Gln859 and wortmannin were broken during at least half of the simulation time. This implies that Gln859 may not be as significant as Ser774 for mutant-specific ligand binding. Further investigation of residue Gln859 showed that it played a significant role in maintaining the H-bond network of the binding pocket; the distance between the Gln859 backbone NH and the Thr856 side chain OH was stable at 2.2 ± 0.3 Å in the MUT model, whereas the same distance in the wt model was 3.1 ± 1.2 Å (Figure 4D). The favorable interactions of Ser774 and Gln859 for ligand binding to the H1047R mutant PI3Kα were also observed in our previous docking studies.[12] Therefore, it is critical to take into account residues Ser774 and Gln859 for ligand design targeting H1047R MUT.

The electrostatic potential surface maps of the WT and MUT PI3Kα proteins with the RESP and QPLD charge models provided further evidence of the role of Ser774 and Gln859 in mutant-specific ligand binding. The commonality between the four PI3Kα models are Asp933 and Val851, two important residues discussed elsewhere.[11,12] Ser774 was observed in all PI3Kα models except for the WT models (Figure 5), in accord with the H-bond patterns shown in Figure 1. Similarly, Gln859 formed a stable H-bond with Thr856 of 3HHM, whereas Gln859 was not even observed in the active site of the WT QPLD model (2RD0). Another difference between the wt and

dx.doi.org/10.1021/ci3003057 | J. Chem. Inf. Model. 2012, 52, 3213−3224

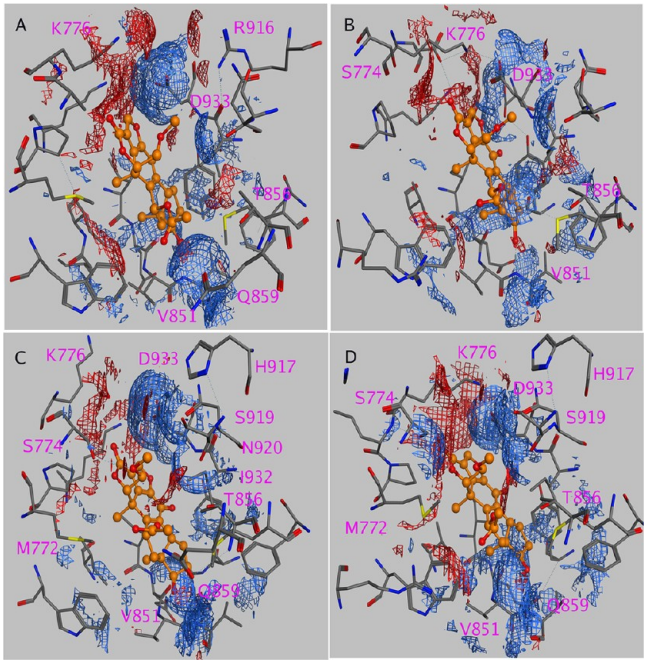

Figure 5. Electrostatic surface of the binding pockets of (A) wt PI3Kα (RESP model); (B) wt PI3Kα (QPLD model); (C) MUT PI3Kα (RESP model); and (D) MUT PI3Kα (QPLD model). Color code: H-bond acceptor, red; and H-bond donor, blue. The electrostatic surfaces were made with the MOE program.

MUT PI3Kα is the H-bond network in the binding pocket. In the MUT models, His917 forms H-bonds with Ser919, a polar residue that forms a dipole−dipole interaction with the carbonyl group of the wortmannin (Figure 5D). In the WT PI3Kα model, Arg916 forms H-bonds with Asp933, another residue important for ligand binding. Neither Arg916 nor His917 were observed in the fourth ns snapshot of the WT QPLD model. We suggest that H1047R mutant specific inhibitors would be particularly useful for treating colon and breast cancer patients, 30% of whom carry the H1047R mutation; such inhibitors might also minimize side effects arising from inhibiting wild-type PI3Kα. However, inhibiting wild-type PI3Kα may be important for cancer types such as gastric cancer where overexpression of WT PI3Kα is observed.

Sequence alignment between PI3Kα and PI3Kγ showed that Ser774, Val851, Gln859, and Asp933 of PI3Kα correspond to residues Ser806, Val882, Lys890, and Asp964 of PI3Kγ (for the whole sequence alignment, refer to reference 12 in the Supporting Information). An electrostatic potential surface shows that Gln859 in the PI3Kα model is a H-bond donor (blue region, Figure 5) whereas Lys890 is a H-bond acceptor (red region, Figure 3). The position of Gln859 in PI3Kα does play a role in ligand selectively binding to PI3Ks (the residues at this position is Lys890 in PI3Kγ, and Asn836 in PI3Kδ[42,43]). Figure 5 also shows that Lys776 is important for ligand binding to the α isoform since it provides a stabilizing H-bond interaction with Asp933. The corresponding residue in PI3Kγ is Lys808, absent from the 4.5 Å interacting pocket. The ammonium group (NH_3^+) of Lys890 adopts an extended conformation in the active site of PI3Kγ (QPLD model), making it possible to serve as two H-bond acceptors (one from the side chain NH_3^+, one from the main chain carbonyl oxygen). However, the same residue in the RESP model pointed away from the binding site, allowing only one H-bond interaction with the backbone carbonyl group (Figure 3).

Therefore, although the overall RMSDs are similar between the RESP and QPLD charge models, individual residues, particularly those interacting with ligands, behave quite differently. The QPLD model, with improved prediction of electrostatic interactions, is able to reproduce the experimentally determined $\Delta G_{bind.}$ The overall free energies of binding in the H1047R mutant PI3Kα model and in the γ model between RESP and QPLD charge systems are comparable and in accord with experimental values.

3.4. Hot Spot Residues at the Binding Interfaces Unraveled by Computational Alanine Scanning. Hot spot residues in each interface were identified with the MM/GBSA method by mutating binding residues to alanine and comparing binding free energies of the mutants to that of the original protein. $\Delta\Delta G_{bind}$ is defined as ΔG_{bind} (alanine mutant) − ΔG_{bind} (wild-type). A positive $\Delta\Delta G_{bind}$ indicates an unfavorable mutation, that is, a ligand binds more favorably to the WT. In other words, a residue with a large positive $\Delta\Delta G_{bind}$ indicates that it is critical for ligand binding. On the other hand, a negative $\Delta\Delta G_{bind}$ indicates a preference for the alanine mutant, that is, a ligand binds more favorably to the mutant. The proline residue was not mutated because of its usual backbone conformation; replacing proline with alanine induces significant conformational changes and thus affects the binding mode.[44]

PIK3CA mutations can be used to predict resistance to two monoclonal antibodies (cetuximab and panitumumab) for suppressing epidermal growth factor receptor (EGFR) in metastatic colorectal cancer (mCRC) patients.[45] In patients with KRAS wild-type mCRC, a lower objective response rate was observed in patients with PIK3CA exon 20 mutations.[46] Among 377 patients, 62% carried WT KRAS and 38% with KRAS mutations. In both the KRAS WT and mutants group, 89% of patients of mCRC have WT PIK3CA whereas 11% carried PIK3CA mutations.[46] A study of important binding residues in the WT and MUT PI3Kα, therefore, is fundamental for mutant- or isoform-specific ligand design.

To determine the role of each binding residue in ligand binding to the wild-type or H1047R mutant of PI3Kα, or PI3Kγ, we systematically applied computational alanine scanning to PI3Ks active site residues. The binding free energies ($\Delta\Delta G_{subtot}$) of WT PI3Kα (QPLD charge model, Table 3) show that significant losses in the binding free energies were observed for the hydrophobic Val851, and Val850. In addition, the hydrophobic Trp780, Ile800, Tyr836, I848, Met922, and Ile932 showed $\Delta\Delta G_{subtot}$ increases of greater than 2.5 kcal/mol. This indicates that a mutation of any of these residues would weaken ligand binding. Therefore, Trp780, Ile800, Tyr836, I848, Val850, Val851, Met922, and Ile932 can be called "resistant" mutants or "hot-spot" residues. This agrees with the energetic analysis of the binding free energies where van der Waals interactions are dominant. The prediction of Ile848 being an important binding residue ($\Delta\Delta G_{subtot}$ of 4.1 kcal/mol) was corroborated by experimental observations that the mutant I848A possesses severely impaired enzyme activity (>100 fold weaker than the WT PI3Kα).[14] These data shows that these residues are significant for ligand/protein interactions.

Inspection of individual energy components (Table 3) of these mutations in the QLPD model shows that losses in hydrophobic interactions ($\Delta\Delta E_{vdw}$) contribute the most to the $\Delta\Delta G_{subtot}$, the relative energy of binding without the entropy

dx.doi.org/10.1021/ci3003057 | J. Chem. Inf. Model. 2012, 52, 3213−3224

Table 3. Relative Free Energies of Binding (kcal/mol) for PI3K Alanine Mutants ($\Delta\Delta G_{subtot} = \Delta G_{mutant} - \Delta G_{wt}$) for the 2RD0 (WT QPLD model)[a]

residues	$\Delta\Delta E_{elec}$	$\Delta\Delta E_{vdw}$	$\Delta\Delta G_{SA}$	$\Delta\Delta G_{GB}$	$\Delta\Delta G_{solv}$	$\Delta\Delta G_{subtot}$
M772	1.2	1.3	0.2	−1.2	−1.0	1.5
S774	0.4	0.7	0.1	−0.7	−0.6	0.5
K776	0.9	1.2	0.2	−1.3	−1.2	1.0
W780	5.0	4.0	0.6	−5.2	−4.6	4.5
I800	3.6	2.2	0.3	−3.3	−3.0	2.8
Y836	8.2	3.6	0.3	−8.2	−7.9	3.9
I848	3.6	3.6	0.4	−3.5	−3.1	4.1
E849	5.3	0.9	0.1	−4.9	−4.8	1.4
V850	1.4	0.8	0.0	7.7	7.7	9.9
V851	1.3	0.5	0.0	8.4	8.4	10.1
T856	−0.3	0.5	0.1	0.3	0.4	0.5
Q859	4.0	1.3	0.2	−4.3	−4.1	1.2
H917	0.4	0.0	0.0	−0.1	−0.1	0.4
M922	2.1	2.3	0.3	−1.8	−1.5	2.8
I932	3.2	4.5	0.3	−3.3	−3.0	4.7
D933	−0.8	1.6	0.1	0.7	0.8	1.5
D933/F934	−1.4	1.8	0.1	1.2	1.3	1.7
E970	1.5	0.0	0.0	−1.1	−1.1	0.4

[a]The energy components and standard deviations are listed in Supporting Information Table 3S.

component. One assumption of computational alanine scanning is that replacing the original residues with an alanine will cause only small local changes that have little effect on entropy, that is, the entropic terms ($-T\Delta S$) for the wild-type and the mutants should cancel out. The predominant factor for V850A and V851A is solvation energy loss ($\Delta\Delta G_{solv}$). For polar residues Tyr836, Glu849, Gln859, Met922, and Glu970, mutations to alanine lead to loss of electrostatic interactions (positive $\Delta\Delta E_{elec}$). A comparison of wild-type (2RD0) with H1047R mutant (3HHM) under the same QPLD model shows that Val850 and Val851 are important for ligand binding (Figure 6A), whereas the role of these two residues diminishes in the ligand binding toward H1047R mutant (Figure 6B).

To identify residues responsible for mutant-specific binding, we applied the same MM/GBSA method to binding residues in MUT H1047R PI3Kα (Table 4). Compared to the WT PI3Kα, these mutations should be considered as double mutations. Data in Table 4 and Figure 6B show that in the MUT PI3Kα model, Ile932, Trp780, Tyr836, and Met922 are residues critical for ligand binding to the MUT isoform. Similar to the WT model, losses in $\Delta\Delta E_{vdw}$ predominate for Trp780, Tyr836, and Met922. Although Ser774 $\Delta\Delta E_{subtot}$ in both the WT and MUT is less than 1 kcal/mol, the individual $\Delta\Delta E_{elec}$ energy components of 0.4 and 8.6 kcal/mol for the WT and MUT isoforms are quite different. As shown in Figure 4B, this may correspond to the loss of H-bonds in the MUT models.

The main difference between the WT and MUT hot spot residues lies in Val850, Val851, and Ile932. Val850 and Val851 were predicted to be important in the WT (QPLD models), whereas Ile932 was predicted to be more critical in the H1047R mutant. In the MUT model, the $\Delta\Delta E_{subtot}$ of Ile932 was predicted to be 3.8 kcal/mol in the RESP model, and 11.7 kcal/mol in the QPLD model. In the WT QPLD charge model, the $\Delta\Delta E_{subtot}$ of Ile932 became 4.7 kcal/mol. Under the QPLD charge model, Val851 appears to be more WT-specific and Ile932 more MUT-specific. Val850, on the other hand, is important to WT, but not to MUT ligand binding in both charge models. An inspection of the Ile932 interaction network shows that the Ile932 backbone NH in the QPLD MUT model formed a H-bond with side chain amide group of Asn920, stabilizing the binding pocket of MUT model (Figure 5C). Similar to Ser774, the increase in $\Delta\Delta E_{elec}$ may be attributed to the loss of a H-bond stabilizing effect. Excluding Ile932, the correlation (R^2) of the $\Delta\Delta E_{subtot}$ between the QPLD and RESP models is 0.65 (Supporting Information Figure 2SA), suggesting both charge models would be able to predict the mutational effect of PI3Kα.

To validate the MM/GBSA calculations in the MUT model, we performed double-mutations on the WT PI3Kα, and compared the $\Delta\Delta G_{subtot}$ of these mutants to those of the H1047R MUT model. Our data showed that these two set of data yield a similar trend (Table 5). The linear relationship of the $\Delta\Delta G_{subtot}$ between these two models (R^2 of 0.69, Supporting Information Figure 2SB) further verified the reliability of using computational alanine scanning to predict the residue behaviors. The validation of double mutational effects can also be illustrated in the D933A/F934A mutant: the

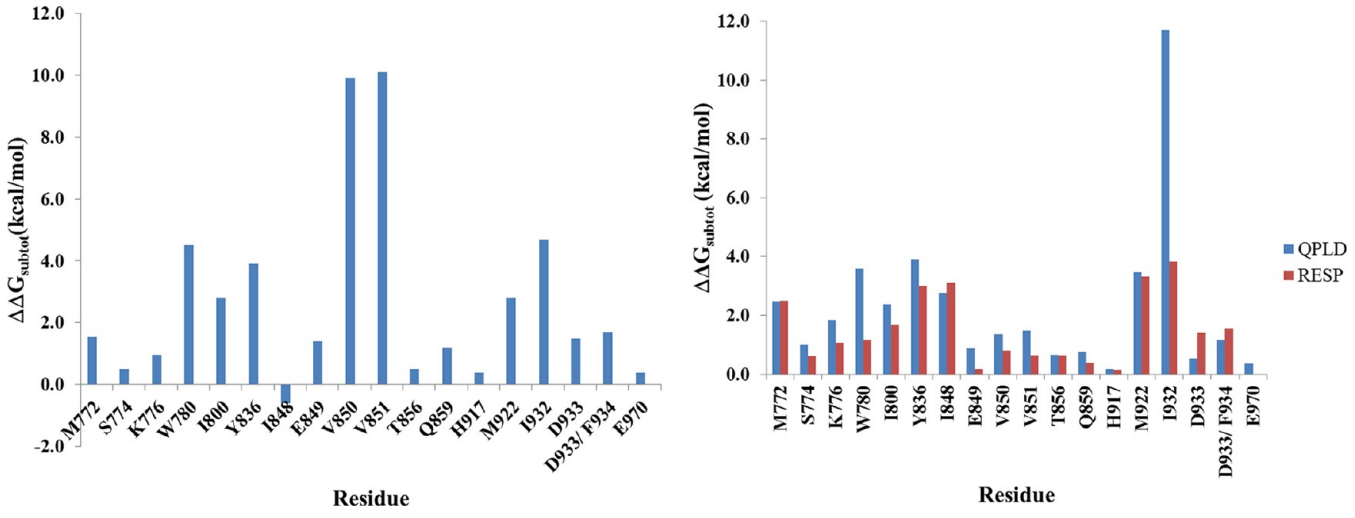

Figure 6. MM/GBSA binding free energy for (A) WT PI3Kα (2RD0, QPLD model) and (B) H1047R MUT PI3Kα (3HHM, both QPLD and RESP models).

dx.doi.org/10.1021/ci3003057 | J. Chem. Inf. Model. 2012, 52, 3213−3224

Table 4. Relative Binding Free Energies (kcal/mol) for PI3K Alanine Mutants ($\Delta\Delta G_{subtot} = \Delta G_{mutant} - \Delta G_{wt}$) for the 3HHM MUT models (QPLD model)[a]

residues	$\Delta\Delta E_{elec}$	$\Delta\Delta E_{vdw}$	$\Delta\Delta G_{SA}$	$\Delta\Delta G_{GB}$	$\Delta\Delta G_{solv}$	$\Delta\Delta G_{subtot}$ QPLD	$\Delta\Delta G_{subtot}$ RESP
M772	3.3	2.3	0.4	−3.6	−3.2	2.5	2.5
S774	8.6	−1.0	0.0	−6.6	−6.6	1.0	0.6
K776	−2.8	0.9	0.1	3.7	3.7	1.8	1.1
W780	0.2	2.8	0.3	0.2	0.6	3.6	1.2
I800	0.6	1.9	0.2	−0.4	−0.1	2.4	1.7
Y836	1.7	2.8	0.2	−0.8	−0.6	3.9	3.0
I848	−0.5	2.1	0.2	0.9	1.1	2.8	3.1
E849	3.0	0.1	0.0	−2.2	−2.2	0.9	0.2
V850	−0.7	0.8	0.0	1.2	1.3	1.4	0.8
V851	−0.7	0.6	0.0	1.6	1.6	1.5	0.6
T856	−0.5	0.5	0.1	0.5	0.6	0.6	0.6
Q859	−1.2	0.3	0.0	1.6	1.7	0.8	0.4
H917	0.4	0.2	0.0	−0.4	−0.4	0.2	0.1
M922	0.7	2.2	0.3	0.3	0.6	3.5	3.3
I932	−6.6	3.3	0.2	14.9	15.1	11.7	3.8
D933	−1.5	1.1	0.2	0.8	1.0	0.5	1.4
D933/F934	−0.8	1.6	0.2	0.2	0.3	1.2	1.6
E970	1.5	0.0	0.0	−1.1	−1.1	0.4	0.0

[a]The energy components and standard deviations are listed in Supporting Information Tables 5S−7S.

Table 5. Relative Free Energies of Binding (kcal/mol) for Double Mutants (Alanine Mutants of PI3Kα Binding Residue Plus H1047R MUT, QPLD Model)[a]

residues	$\Delta\Delta E_{elec}$	$\Delta\Delta E_{vdw}$	$\Delta\Delta G_{SA}$	$\Delta\Delta G_{GB}$	$\Delta\Delta G_{solv}$	$\Delta\Delta G_{subtot}$ QPLD (double mutant)	$\Delta\Delta G_{subtot}$ QPLD (3HHM)
E849 + H1047	3.6	0.1	0.0	−3.1	−3.1	0.6	0.9
D933 + H1047	−1.4	1.6	0.1	1.2	1.3	1.4	0.5
I848 + H1047	2.5	2.8	0.3	−2.0	−1.7	3.5	2.8
I800 + H1047	1.4	1.4	0.2	−1.0	−0.8	1.9	2.4
Y836 + H1047	5.0	3.0	0.2	−5.2	−5.0	2.9	3.9
W780 + H1047	2.3	3.0	0.4	−2.5	−2.1	3.2	3.6
V851 + H1047	1.1	0.5	0.0	−1.1	−1.1	0.5	1.5
V850 + H1047	1.6	0.8	0.0	−1.7	−1.7	0.7	1.4

[a]The $\Delta\Delta G_{subtot}$ values from the QPLD (3HHM model, Table 4) are listed for comparison. The energy components and standard deviations are listed in Supporting Information Table 8S.

$\Delta\Delta G_{subtot}$ for this double mutant in the WT QPLD model is 1.7 kcal/mol (Table 3), suggesting an adverse effect of this double mutant, consistent with a complete loss of enzymatic activity of the double mutant D933A/F934A.[13] Zunder et al.[15] observed that mutants I800L, I800M, and I848V required 10-fold or higher concentrations to reach the enzymatic activity of the H0147R mutant, indicating that mutations on residues I800 and I848 of MUT H0147R are not favorable. Our calculations of I800A and I848A in the MUT model (2.4 and 2.8 kcal/mol, respectively, Table 4) and in the double mutant WT model (1.9 and 3.5 kcal/mol, respectively, Table 5) further confirm the unfavorable mutation of these two residues. These two residues, however, may not be mutant-specific in that the $\Delta\Delta G_{subtot}$s were very close for both the WT and MUT models (Table 4). Therefore, MM/GBSA alanine scanning suggests that Ile932 and Ser774 might be mutant-specific.

To identify residues responsible for isoform-specific binding, we applied computational alanine scanning to PI3Kγ residues Ser806, Trp812, Ile831, Tyr867, Ile879, Ile881, Val882, Thr886, Lys890, and Asp964, corresponding to PI3Kα residues Ser774, Trp780, Ile800, Tyr836, Ile848, Val850, Val851, His855, Gln859, and Asp933, respectively. Figure 7 suggests that Ile831, Ile879, Trp812, and Lys890 are residues critical for ligand binding to PI3Kγ. For PI3Kγ, the QPLD charge model generally yielded a better $\Delta\Delta G_{subtot}$ than the RESP charge model. However, both charge models showed similar trends with a correlation of 0.73 (R^2, Figure 7B). As Trp812, Ile831, and Ile879 of PI3Kγ provide important hydrophobic interactions for ligand binding, so do Trp780, Ile800, and I848 for PI3Kα. Therefore, these three residues may not be isoform-specific.

Alanine scanning of residues in PI3Kγ showed that the QPLD model predicted four residues (Trp812, Ile831, Ile879, and Lys890) to be important for ligand binding, whereas the RESP charge model predicted only two (Trp812 and Ile831). Data in Figures 2 and 3 confirmed the importance of Lys890. According to the QPLD charge model, Lys890 of PI3Kγ is predicted to be important for ligand binding ($\Delta\Delta G_{subtot}$ of 3.5 kcal/mol, Supporting Information Table 9S). Data in Figure 3 shows that Lys890 in the QPLD-generated MD trajectory had two H-bond acceptor regions, while it had only one in the RESP charge model (which had a $\Delta\Delta G_{subtot}$ of 0 kcal/mol, Supporting Information Table 10S). According to site-directed mutagenesis,[47] Lys890 is a residue proven to be important for

dx.doi.org/10.1021/ci3003057 | J. Chem. Inf. Model. 2012, 52, 3213−3224

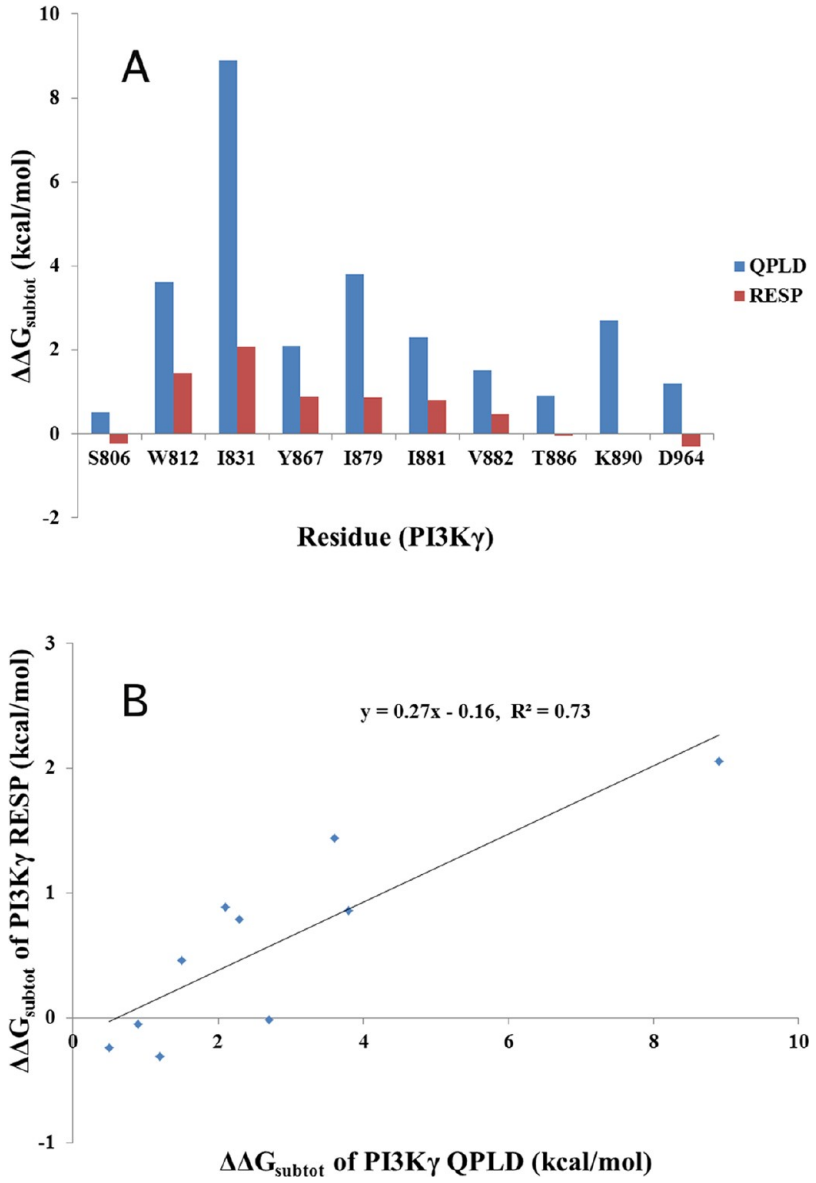

Figure 7. MM/GBSA binding free energy for PI3Kγ (A), and the correlation between the QPLD and RESP charge models for PI3Kγ (B). The energy components and standard deviations of 1E7 V/LY294002 interactions are listed in Supporting Information Tables 9S and 10S.

ligand binding to PI3Kγ. The amino group of Lys890 is oriented toward the binding cleft and therefore can form a stronger electrostatic interaction with wortmannin. In addition, the Lys890 main chain NH forms a H-bond with side chain hydroxyl group of Thr886 (Figure 8B). The corresponding residue in the α isoform is Gln859, which might be important for mutant-selective binding due to forming H-bonds with Thr856 (Figure 4D). For the WT PI3Kα, such a H-bond is not stable due to its distance from the active site (not within the 4.5 Å of bound ligand, Figures 5B, and 8A), Gln859 may not be critical for ligand binding to the α isoform and yet the corresponding residue in PI3Kγ (Lys890) is important for binding. Therefore, Lys890 may be isoform-specific.

4. CONCLUSIONS

We applied molecular dynamics (MD) simulations to the WT and MUT PI3Kα and PI3Kγ based on RESP (restrained electrostatic potential) and quantum mechanics (QM)-polarized ligand docking (QPLD)-derived partial charges. The PI3K QPLD and RESP charge models show similar performance in MD simulations in terms of maintaining the stability of the aqueous systems. However, individual residues do behave differently, particularly for residues critical for mutant- or isoform-specific binding. We applied the GBSA method to estimate the binding free energies of wortmannin to PI3Kα and, LY294002 to PI3Kγ. The binding free energies of LY294002 to PI3Kγ models (−9.3 and −9.5 kcal/mol) are in a very good agreement with the experiment (−9.2 kcal/mol), and the binding free energies of wortmannin to PI3Kα models (−11.7 and −10.9) also agree with observed data (−10.9 kcal/mol). MM/GBSA calculations suggested that residues Ser774, Gln859, and Ile932 might be used to design PI3Kα mutant-specific ligands, whereas Lys890 can be used for PI3Kγ ligand design.

dx.doi.org/10.1021/ci3003057 | J. Chem. Inf. Model. 2012, 52, 3213−3224

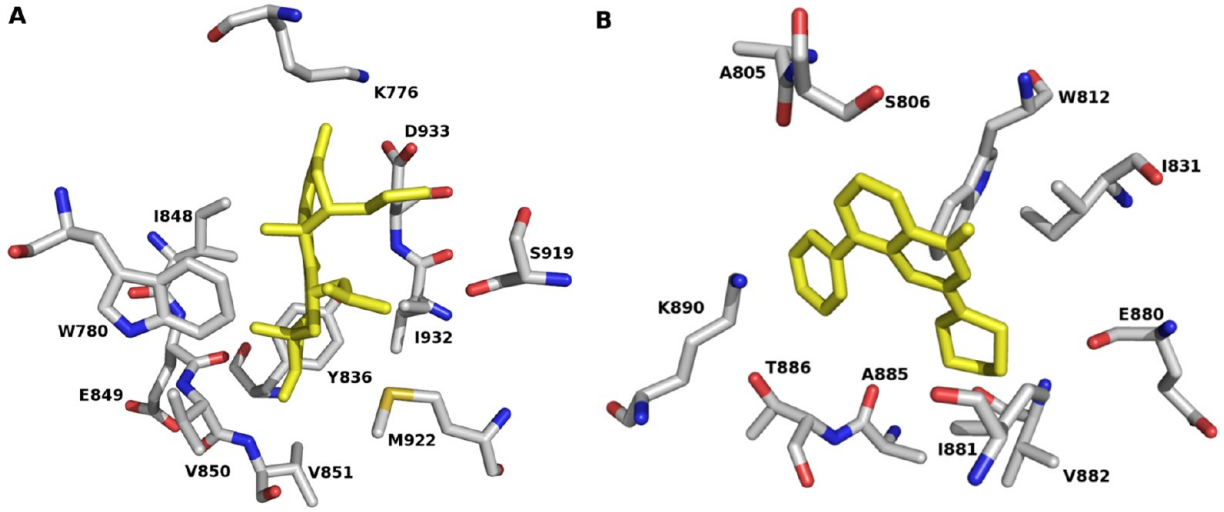

Figure 8. Binding pockets of (A) 2RD0 and (B) 1E7V. Ligands are represented in yellow color. Hydrogen atoms are hidden for clarity purpose.

■ ASSOCIATED CONTENT

Supporting Information

Atom types and atomic partial charges of wortmannin and LY294002 and binding free energy components along with standard deviations for MD simulation models. This material is available free of charge via the Internet at http://pubs.acs.org.

■ AUTHOR INFORMATION

Corresponding Author

*Tel. +1 402 554 3145. Fax: +1 402 554-3888. E-mail: hzhong@unomaha.edu.

Present Address

Current address for Dima A. Sabbah: College of Pharmacy, Al-Zaytoonah Private University of Jordan, P.O. Box 130, Amman 11733, Jordan.

Notes

The authors declare no competing financial interest.

■ ACKNOWLEDGMENTS

This work was partially supported by the Research Corporation for Science Advancement. DAS acknowledges Al-Zaytoonah Private University of Jordan for financial support, and a Bukey Fellowship from the University of Nebraska Medical Center.

■ REFERENCES

(1) Vivanco, I.; Sawyers, C. L. The phosphatidylinositol 3-kinase-AKT pathway in human cancer. *Nat. Rev. Cancer* **2002**, *2*, 489−501.

(2) Sabbah, D. A.; Brattain, M. G.; Zhong., H. Dual inhibitors of PI3K/mTOR or mTOR-selective inhibitors: Which way shall we go? *Curr. Med. Chem.* **2011**, *18*, 5528−5544.

(3) Rueckle, T.; Schwarz, M. K.; Rommel, C. PI3K gamma inhibition: Towards an "aspirin of the 21st century". *Nat. Rev. Drug Discovery* **2006**, *5*, 903−918.

(4) Samuels, Y.; Wang, Z.; Bardelli, A.; Silliman, N.; Ptak, J.; Szabo, S.; Yan, H.; Gazdar, A.; Powell, D.; Riggins, G.; Willson, J.; Markowitz, S.; Kinzler, K.; Vogelstein, B.; Velculescu, V. High frequency of mutations of the PIK3CA gene in human cancers. *Science* **2004**, *304*, 554−554.

(5) Liu, P.; Cheng, H.; Roberts, T. M.; Zhao, J. J. Targeting the phosphoinositide 3-kinase pathway in cancer. *Nat. Rev. Drug Discovery* **2009**, *8*, 627−644.

(6) Mandelker, D.; Gabelli, S.; Schmidt-kittler, O.; Zhu, J.; Cheong, I.; Huang, C. H.; Kinzler, K.; Vogelstein, B.; Amzel, M. A frequent kinase domain mutation that changes the interaction between PI3KR and the membrane. *Proc. Natl. Acad. Sci. U. S. A.* **2009**, *106*, 16996−17001.

(7) Kang, S. Y.; Bader, A. G.; Vogt, P. K. Phosphatidylinositol 3-kinase mutations identified in human cancer are oncogenic. *Proc. Natl. Acad. Sci. U. S. A.* **2005**, *102*, 802−807.

(8) Liu, Z. N.; Roberts, T. M. Human tumor mutants in the p110 alpha subunit of PI3K. *Cell Cycle* **2006**, *5*, 675−677.

(9) Shi, J.; Yao, D.; Liu, W.; Wang, N.; Lu, H.; Zhang, G.; Ji, M.; Xu, L.; He, N.; Shi, B.; Hou, P. Highly frequent PIK3CA amplification is associated with poor prognosis in gastric cancer. *BMC Cancer* **2012**, *12*, No. 50.

(10) Vermaat, J. S.; Nijman, I. J.; Koudijs, M. J.; Gerritse, F. L.; Scherer, S. J.; Mokry, M.; Roessingh, W. M.; Lansu, N.; De Bruijn, E.; Van Hillegersberg, R.; Van Diest, P. J.; Cuppen, E.; Voest, E. E. Primary colorectal cancers and their subsequent hepatic metastases are genetically different: Implications for selection of patients for targeted treatment. *Clin. Cancer Res.* **2012**, *18*, 688−699.

(11) Han, M.; Zhang, J. Z. H.; Class, I. Phospho-inositide-3-kinases (PI3Ks) isoform-specific inhibition study by the combination of docking and molecular dynamics simulation. *J. Chem. Inf. Model.* **2010**, *50*, 136−145.

(12) Sabbah, D. A.; Vennerstrom, J. L.; Zhong, H. Docking studies on isoform-specific inhibition of phosphoinositide-3-kinases. *J. Chem. Inf. Model.* **2010**, *50*, 1887−1898.

(13) Stirdivant, S. M.; Ahern, J.; Conroy, R. R.; Barnett, S. F.; Ledder, L. M.; Oliff, A.; Heimbrook, D. C. Cloning and mutagenesis of the p110 alpha subunit of human phosphoinositide 3′-hydroxykinase. *Bioorg. Med. Chem.* **1997**, *5*, 65−74.

(14) Alaimo, P. J.; Knight, Z. A.; Shokat, K. M. Targeting the gatekeeper residue in phosphoinositide 3-kinases. *Bioorg. Med. Chem.* **2005**, *13*, 2825−2836.

(15) Zunder, E. R.; Knight, Z. A.; Houseman, B. T.; Apsel, B.; Shokat, K. M. Discovery of drug-resistant and drug-sensitizing mutations in the oncogenic PI3K isoform p110α. *Cancer Cell* **2008**, *14*, 180−192.

(16) Huang, C.; Mandelker, D.; Schmidt-Kittler, O.; Samuels, Y.; Velculescu, V. E.; Kinzler, K. W.; Vogelstein, B.; Gabelli, S. B.; Amzel, L. M. The structure of a human p110 alpha/p85 alpha complex elucidates the effects of oncogenic PI3K alpha mutations. *Science* **2007**, *318*, 1744−1748.

(17) Massova, I.; Kollman, P. A. Computational alanine scanning to probe protein-protein interactions: A novel approach to evaluate binding free energies. *J. Am. Chem. Soc.* **1999**, *121*, 8133−8143.

(18) Zhong, H. Z.; Carlson, H. A. Computational studies and peptidomimetic design for the human p53-MDM2 complex. *Proteins: Struct., Funct., Bioinf.* **2005**, *58*, 222−234.

(19) Cho, A. E.; Guallar, V.; Berne, B. J.; Friesner, R. Importance of accurate charges in molecular docking: Quantum mechanical/molecular mechanical (QM/MM) approach. *J. Comput. Chem.* **2005**, *26*, 915−931.
(20) Zhong, H.; Kirschner, K. N.; Lee, M.; Bowen, J. P. Binding free energy calculation for duocarmycin/DNA complex based on the QPLD-derived partial charge model. *Bioorg. Med. Chem. Lett.* **2008**, *18*, 542−545.
(21) Walker, E. H.; Pacold, M. E.; Perisic, O.; Stephens, L.; Hawkins, P. T.; Wymann, M. P.; Williams, R. L. Structural determinants of phosphoinositide 3-kinase inhibition by wortmannin, LY294002, quercetin, myricetin, and staurosporine. *Mol. Cell* **2000**, *6*, 909−919.
(22) *The Molecular Operating Environment (MOE)*; Chemical Computing Group Inc.; Montreal, Quebec, Canada, 2009.
(23) Frisch, M. J.; Trucks, G. W.; Schlegel, H. B.; Scuseria, G. E.; Robb, M. A.; Cheeseman, J. R.; Montgomery, J., J. A.; Vreven, T.; Kudin, K. N.; Burant, J. C.; Millam, J. M.; Iyengar, S. S.; Tomasi, J.; Barone, V.; Mennucci, B.; Cossi, M.; Scalmani, G.; Rega, N.; Petersson, G. A.; Nakatsuji, H.; Hada, M.; Ehara, M.; Toyota, K.; Fukuda, R.; Hasegawa, J.; Ishida, M.; Nakajima, T.; Honda, Y.; Kitao, O.; Nakai, H.; Klene, M.; Li, X.; Knox, J. E.; Hratchian, H. P.; Cross, J. B.; Bakken, V.; Adamo, C.; Jaramillo, J.; Gomperts, R.; Stratmann, R. E.; Yazyev, O.; Austin, A. J.; Cammi, R.; Pomelli, C.; Ochterski, J. W.; Ayala, P. Y.; Morokuma, K.; Voth, G. A.; Salvador, P.; Dannenberg, J. J.; Zakrzewski, V. G.; Dapprich, S.; Daniels, A. D.; Strain, M. C.; Farkas, O.; Malick, D. K.; Rabuck, A. D.; Raghavachari, K.; Foresman, J. B.; Ortiz, J. V.; Cui, Q.; Baboul, A. G.; Clifford, S.; Cioslowski, J.; Stefanov, B. B.; Liu, G.; Liashenko, A.; Piskorz, P.; Komaromi, I.; Martin, R. L.; Fox, D. J.; Keith, T.; Al-Laham, M. A.; Peng, C. Y.; Nanayakkara, A.; Challacombe, M.; Gill, P. M. W.; Johnson, B.; Chen, W.; Wong, M. W.; Gonzalez, C. *Gaussian 03*, revision C.02; Gaussian, Inc.: Wallingford, CT, 2004.
(24) Case, D. A.; Darden, D. A.; Cheatham, I., T. E.; Simmerling, C. L.; Wang, J.; Duke, R. E.; Luo, R.; Crowley, M.; Walker, R. C.; Zhang, W.; Merz, K. M.; Wang, B.; Hayik, S.; Roitberg, A.; Seabra, G.; Kolossvàry, I.; Wong, K. F.; Paesani, F.; Vanicek, J.; Wu, X.; Brozell, S. R.; Steinbrecher, T.; Gohlke, H.; Yang, L.; Mongan, J.; Hornak, V.; Kollman, P. A. *AMBER10*; University of California: San Francisco, CA, 2008.
(25) *Protein Preparation Wizard*; *Maestro*; *MacroModel*; *Phase, QM-Based Ligand Docking*; *Glide*; Schrödinger, LLC: Portland, OR, 2009.
(26) Hornak, V.; Abel, R.; Okur, A.; Strockbine, B.; Roitberg, A.; Simmerling, C. Comparison of multiple amber force fields and development of improved protein backbone parameters. *Proteins: Struct., Funct., Bioinf.* **2006**, *65*, 712−725.
(27) Jorgensen, W. L.; Chandrasekhar, J.; Madura, J. D.; Impey, R. W.; Klein, M. L. Comparison of simple potential functions for simulating liquid water. *J. Chem. Phys.* **1983**, *79*, 926−935.
(28) Darden, T.; York, D.; Pedersen, L. Particle mesh Ewald—An *N*·log(*n*) method for Ewald sums in large systems. *J. Chem. Phys.* **1993**, *98*, 10089−10092.
(29) Tsui, V.; Case, D. A. Molecular dynamics simulations of nucleic acids with a generalized Born solvation model. *J. Am. Chem. Soc.* **2000**, *122*, 2489−2498.
(30) Bashford, D.; Case, D. A. Generalized Born models of macromolecular solvation effects. *Annu. Rev. Phys. Chem.* **2000**, *51*, 129−152.
(31) Jayaram, B.; Sprous, D.; Beveridge, D. L. Solvation free energy of biomacromolecules: Parameters for a modified generalized Born model consistent with the AMBER force field. *J. Phys. Chem. B* **1998**, *102*, 9571−9576.
(32) Scanner, M. F.; Olson, A. J.; Spehner, J. C. Reduced surface: An efficient way to compute molecular surfaces. *Biopolymers* **1996**, *38*, 305−320.
(33) Case, D. A. Normal-mode analysis of protein dynamics. *Curr. Opin. Struct. Biol.* **1994**, *4*, 285−290.
(34) Kottalam, J.; Case, D. A. Langevin modes of macromolecules—Applications to Crambin and DNA hexamers. *Biopolymers* **1990**, *29*, 1409−1421.
(35) Perdih, A.; Bren, U.; Solmajer, T. Binding free energy calculations of *N*-sulphonyl-glutamic acid inhibitors of MurD ligase. *J. Mol. Model.* **2009**, *15*, 983−996.
(36) Brown, K. L.; Bren, U.; Stone, M. P.; Guengerich, F. P. Inherent stereospecificity in the reaction of aflatoxin B(1) 8,9-epoxide with deoxyguanosine and efficiency of DNA catalysis. *Chem. Res. Toxicol.* **2009**, *22*, 913−917.
(37) Udommaneethanakit, T.; Rungrotmongkol, T.; Bren, U.; Frecer, V.; Stanislav, M. Dynamic behavior of avian influenza A virus neuraminidase subtype H5N1 in complex with oseltamivir, zanamivir, peramivir, and their phosphonate analogues. *J. Chem. Inf. Model.* **2009**, *49*, 2323−2332.
(38) Bren, U.; Hodoscek, M.; Koller, J. Development and validation of empirical force field parameters for netropsin. *J. Chem. Inf. Model.* **2005**, *45*, 1546−1552.
(39) Hon, W. C.; Berndt, A.; Williams, R. L. Regulation of lipid binding underlies the activation mechanism of class IA PI3-kinases. *Oncogene* **2012**, *31*, 3655−3666.
(40) Bren, U.; Martínek, V.; Florián, J. Decomposition of the solvation free energies of deoxyribonucleoside triphosphates using the free energy perturbation method. *J. Phys. Chem. B.* **2006**, *110*, 12782−12788.
(41) Bren, M.; Florián, J.; Mavri, J.; Bren, U. Do all pieces make a whole? Thiele cumulants and the free energy decomposition. *Theor. Chem. Acc.* **2007**, *117*, 535−540.
(42) Murray, J. M.; Sweeney, Z. K.; Chan, B. K.; Balazs, M.; Bradley, E.; Castanedo, G.; Chabot, C.; Chantry, D.; Flagella, M.; Goldstein, D. M.; Kondru, R.; Lesnick, J.; Li, J.; Lucas, M. C.; Nonomiya, J.; Pang, J.; Price, S.; Salphati, L.; Safina, B.; Savy, P. P.; Seward, E. M.; Ultsch, M.; Sutherlin, D. P. Potent and highly selective benzimidazole inhibitors of PI3-kinase delta. *J. Med. Chem.* **2012**, *55*, 7686−7695.
(43) Berndt, A.; Miller, S.; Williams, O.; Le, D. D.; Houseman, B. T.; Pacold, J. I.; Gorrec, F.; Hon, W. C.; Liu, Y.; Rommel, C.; Gaillard, P.; Rückle, T.; Schwarz, M. K.; Shokat, K. M.; Shaw, J. P.; Williams, R. L. The p110 delta structure: mechanisms for selectivity and potency of new PI(3)K inhibitors. *Nat. Chem. Biol.* **2010**, *6*, 117−124.
(44) Clackson, T.; Ultsch, M. H.; Wells, J. A.; de Vos, A. M. Structural and functional analysis of the 1:1 growth hormone/receptor complex reveals the molecular basis for receptor affinity. *J. Mol. Biol.* **1998**, *277*, 1111−1128.
(45) Moroni, M.; Veronese, S.; Benvenuti, S.; Marrapese, G.; Sartore-Bianchi, A.; Di Nicolantonio, F.; Gambacorta, M.; Siena, S.; Bardelli, A. Gene copy number for epidermal growth factor receptor (EGFR) and clinical response to antiEGFR treatment in colorectal cancer: a cohort study. *Lancet Oncol.* **2005**, *6*, 279−286.
(46) Mao, C.; Yang, Z. Y.; Hu, X. F.; Chen, Q.; Tang, J. L. PIK3CA exon 20 mutations as a potential biomarker for resistance to anti-EGFR monoclonal antibodies in KRAS wild-type metastatic colorectal cancer: A systematic review and meta-analysis. *Ann. Oncol.* **2012**, *23*, 1518−1525.
(47) Frazzetto, M.; Suphioglu, C.; Zhu, J.; Schmidt-Kittler, O.; Jennings, I. G.; Cranmer, S. L.; Jackson, S. P.; Kinzler, K. W.; Vogelstein, B.; Thompson, P. E. Dissecting isoform selectivity of PI3K inhibitors: the role of non-conserved residues in the catalytic pocket. *Biochem. J.* **2008**, *414*, 383−390.